

Assessing Taiwanese Traffic Policy on Consecutive Holidays through Forecast Reconciliation and Prediction-based Anomaly Detection Techniques

Mahsa Ashouri¹ Frederick Kin Hing Phoa² Marzia A. Cremona^{3,4}

¹Department of Biostatistics, University of Michigan, US

²Institute of Statistical Science, Academia Sinica, Taiwan

³Department of Operations and Decision Systems, Université Laval, Canada

⁴CHU de Québec – Université Laval Research Center, Canada

Abstract

This study examines the Taiwanese highway traffic behavior on consecutive holidays, with the aim of evaluating the Taiwanese freeway bureau's traffic control and management strategies. We propose a prediction-based detection method for finding highway traffic anomalies using reconciled ordinary least squares (OLS) forecasts and bootstrap prediction intervals. Two fundamental features of traffic flow time series – namely, seasonality and spatial autocorrelation – are captured by adding Fourier terms in OLS models, spatial aggregation (as a hierarchical structure mimicking the geographical division in regions, cities, and stations), and a reconciliation step. Our approach, although simple, is able to model complex traffic datasets with reasonable accuracy. Being based on OLS, it is efficient and permits avoiding the computational burden of more complex methods. Analyses of Taiwan's consecutive holidays in 2019, 2020, and 2021 (73 days) showed strong variations in anomalies across different directions and highways. Specifically, we detected some areas and highways comprising a high number of traffic anomalies (north direction-central and southern regions-highways No. 1 and 3, south direction-southern region-highway No.3), and others with generally normal traffic (east and west direction). These results could provide important decision-support information to traffic authorities.

keywords: Traffic flow, hierarchical and grouped forecasting, reconciling forecast, linear regression

1 Introduction

During consecutive holidays in Taiwan, the demand for the national highway is 1.5 to 2 times more than on weekdays¹. To maintain a reasonable quality of service and cope with anticipated traffic spikes during these holidays, the Taiwan freeway bureau implements various freeway controls and management strategies depending on the characteristics of the holidays. Traffic authorities use different strategies for traffic management, such as planning alternative routes, flexible adjustments on signal timing, traffic directing, and enforcement by local police, ramp metering on roads connecting to freeways, and other temporary transport managements². Other management strategies restrict vehicles from accessing the road network based on their occupancy or their license numbers (high-occupancy or odd-even license plate policies, Chu et al., 2015). However, due to the exponential growth of registered motor vehicles in Taiwan³, controlling traffic flow is becoming more and more difficult for traffic authorities, particularly during consecutive holidays.

Data points that deviate from a dataset's normal behavior are known as anomalies or outliers. This study defines anomalies as extreme deviations from prediction models' expected values using estimated prediction intervals. Specifically, we consider as anomalies the points which exceed the upper limit of the prediction intervals. Anomaly detection on highway traffic flow is a vital aspect of intelligent traffic management systems, and it has been discussed thoroughly in recent years. Indeed, anomalies on highways indicate traffic congestion which can be caused by several factors, such as accidents, rush hours, or severe weather conditions. Importantly, early and accurate detection of unusual traffic events can improve smooth traffic flow on the roads, and avoid life and economic losses (Mondal and Rehena, 2020; Tang and Gao, 2005).

There is a vast literature on traffic anomaly detection (see, e.g., the survey in Djenouri et al., 2019). As an example of a recent paper on this subject, Bawaneh and Simon (2019) introduced a new anomaly detection

¹Chinese version reference: www.freeway.gov.tw/Download_File.ashx?id=13014

²www.thb.gov.tw

³tradingeconomics.com/taiwan/car-registrations

algorithm that searches for significant changes in the occupancy’s road traffic time series. In particular, they transformed the time series with a derivative estimation model into a symbolic representation sequence and used a modified z-score to detect the anomalies in the symbolic sequence. Another example is represented by the work of Huang et al. (2018), who suggested a spatiotemporal pattern network architecture to detect traffic system-level anomalies in a batch-processing fashion. They showed that their proposed technique could effectively capture time series features and discover spatial and temporal patterns for the traffic system. Zhang et al. (2016) analyzed the large-scale traffic data by identifying its features for temporal and spatial patterns. They derived an anomaly index to quantify the network traffic in both features. Riveiro et al. (2017) presented a visual framework that can explore and analyze the multidimensional road traffic data. This framework also detects anomalies and shows an explanation of anomalous events. Finally, a complex method for traffic anomaly detection based on deep learning was recently proposed by Aboah (2021). Their approach includes an anomaly detection model followed by a detection and analysis step. The model foundation is YOLOv5, and the second step includes traffic scene background estimation, road mask extraction, and adaptive thresholding. The candidate anomalies obtained by this pipeline are then passed through a decision tree to detect and analyze the final anomalies.

Prediction-based anomaly detection algorithms similar to the one presented in this paper are becoming an essential tool in several fields, beyond traffic and transportation. For example, Hou et al. (2013) computed the forecast for water quality variation tendencies and detected water quality anomalies using the abnormal thresholds of prediction residuals. Another example is presented by Li et al. (2019a), who suggested a voltage prediction-based anomaly detection algorithm for spacecraft storage batteries based on a deep belief network (DBN). Finally, Pang et al. (2018) designed a graphic indicator of the receiver operating characteristic (ROC) curve of prediction interval, which helps to optimize the prediction interval coverage for detecting anomalous events. When this approach is applied to traffic forecast and anomaly detection, one must consider two important characteristic of traffic data, such as seasonality and spatial correlations.

In this paper, we propose a prediction-based method for detecting traffic anomalies by modeling and forecasting hierarchical time series, and we apply it to Taiwanese highways data, specifically focusing on consecutive holidays (e.g., the Chinese new year holiday), for which the government sets plans to control the traffic flow. In particular, we propose to exploit an ordinary least squares (OLS) forecasting model comprising Fourier terms to reflect the seasonality, while geographical aggregation is incorporated through a hierarchical structure of data, along with a reconciliation mechanism. In addition, we propose a block cross-validation approach for daily (24 hours) forecasting to detect anomalies every 24 hours.

The paper is organized as follow. Section 2 briefly presents the main Taiwanese highways and introduces the traffic flow time series analyzed in this work. In Section 3, we outline the proposed methodology for hierarchical and group time series and we detail the model specification for the application to traffic anomaly detection in Taiwanese highways. The results for traffic flow forecast and consecutive holiday anomaly detection are presented in Section 4. Finally, we draw conclusion in Section 5.

2 Taiwanese highways data

The main Taiwanese highway network involves highways 1, including its elevated part (Keelung city - Kaohsiung), 3 (Jijin, Keelung city - Dapengwan, Pingtung county), and 5 (Nangang, Taipei city - Su-ao, Yilan). Figure 1 illustrates these highways on the Taiwan map in northern (Figure 1a), central (Figure 1b), and southern (Figure 1c) regions. Although Taiwanese highway network includes additional highways (as displayed in Figure 1), traffic data are available only for the three main highways mentioned above. There are 335 detectors located on these highways, which are part of the Electronic Tolling Collection (ETC) system obtained from the Taiwan Freeway Bureau MOTC website⁴. Every five minutes, the detectors in the ETC system record the number and type of vehicles which pass through it (Siu et al., 2020). The type of vehicles considered in this study includes cars, small trucks, buses/coaches, big trucks, and tractor-trailers. The data collected by the ETC system are publicly available and can be downloaded from the website of the Taiwan Freeway Bureau, MOTC.

Our study concerns two years and four months of traffic flow in Taiwan, from 2019-01-01 to 2021-04-30, comprising 73 days of consecutive holidays (see Table 1). For computational reasons, as well as for making the series smoother and reduce noise, we aggregated the data in order to obtain hourly time series (consecutive holidays correspond to $73 \times 24 = 1752$ hours). For simplicity, we exclude Highway 5 from our dataset. We also exclude the “all zero” and “mostly zero” ($\geq 80\%$ of zero values) time series – which amounts at around 1% of the total number of series. The final dataset includes 1590 time series at the most disaggregated level (see Subsection 3.1), each with length of 20424 observations.

Figure 2 displays three examples of Taiwan highway hourly traffic time series corresponding to different vehicle types in different regions, stations, and traffic directions (for four months, from 2021-01-10 23:00:00 to

⁴tiscvcloud.freeway.gov.tw/history/TDCS/

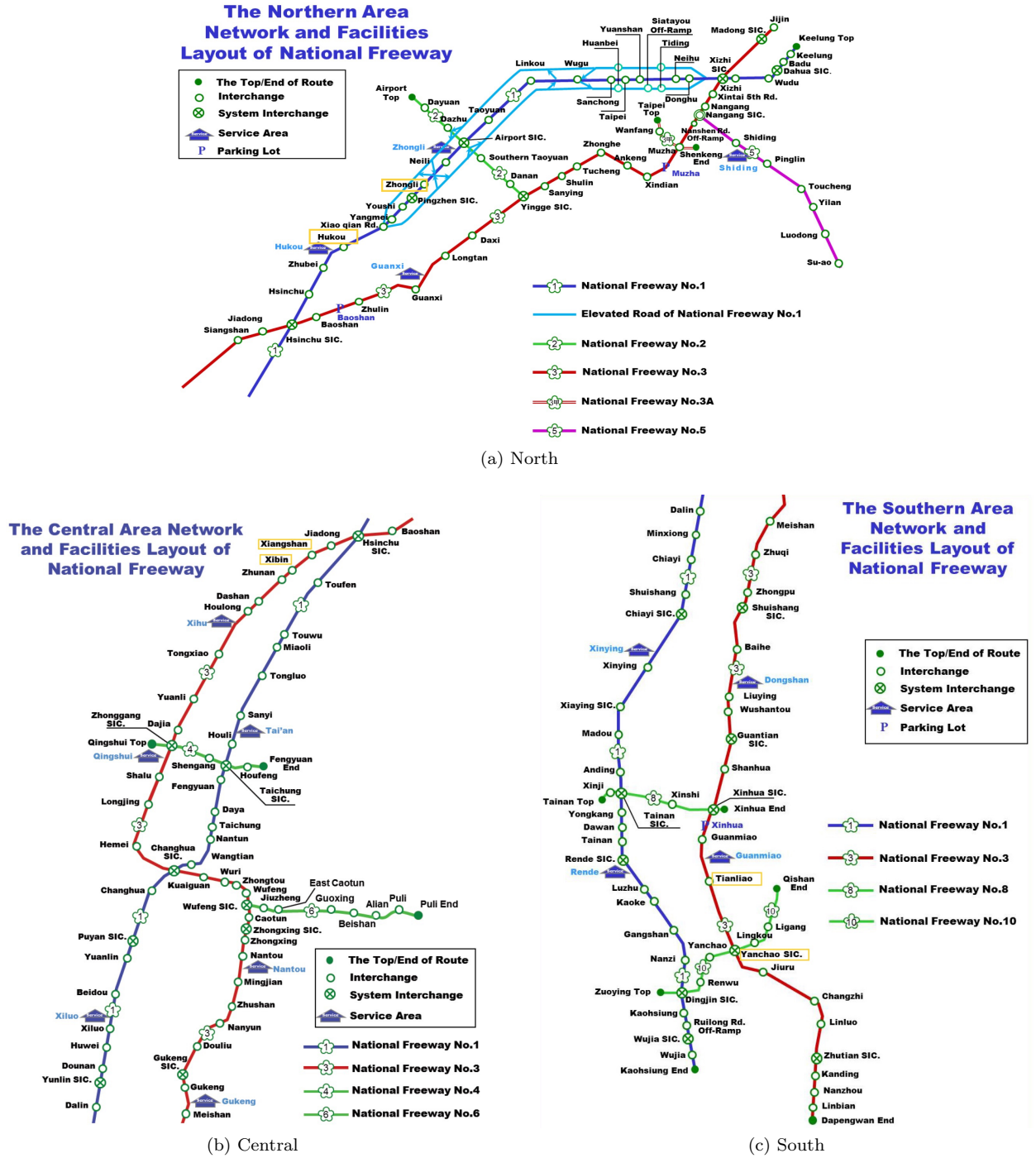


Figure 1: Taiwanese highway network maps in northern, central and southern regions with indication of the sensor stations. Yellow rectangles highlight the sensor stations corresponding to Figures 2 and 3. Figures from www.freeway.gov.tw/english/way_net.aspx?cnid=1110.

2021-04-30 22:00:00). The corresponding sensor stations are highlighted with yellow rectangles in Figure 1. Figure 3 provides a zoomed-in view on the last seven days for the same three time series (hence, from 2021-04-25 23:00:00 to 2021-04-30 22:00:00). In both figures, we can clearly see daily patterns in the Taiwan traffic flow (peak flow in the daytime and much lower flow at night). More in detail, Figure 3 shows that in northern and central regions, the first five days exhibit highly similar daily patterns, with a slightly increased flow on Friday and the weekend. Conversely, in the southern region there is a decrease in big track flow on Friday and Saturday, and a significant drop on Sunday. In addition, we can observe weekly patterns in Taiwan traffic flow (Figure 2). In particular, the weekly patterns in the first four weeks are similar within each time series, while we observe peaks during the fifth week (mid-February) in the series of Figures 2a and 2b, indicating a higher number of cars and small trucks in these highways, respectively. Interestingly, these peaks correspond to a valley in the time series of Figure 2c, which represents the flow

Table 1: Taiwanese consecutive holidays in the time period from 2019-01-01 to 2021-04-30. The last long holiday in the dataset starts on the last day of the time period considered in the study, hence it corresponds to only one day.

Year	Consecutive holidays
2019	02-02 to 02-10 (9 days) 02-28 to 03-03 (4 days) 04-04 to 04-07 (4 days) 06-07 to 06-09 (3 days) 09-13 to 09-15 (3 days) 10-10 to 10-13 (4 days)
2020	01-23 to 01-29 (7 days) 02-28 to 03-01 (3 days) 04-02 to 04-05 (4 days) 05-01 to 05-03 (3 days) 06-25 to 06-28 (4 days) 10-01 to 10-04 (4 days) 10-09 to 10-11 (3 days)
2021	01-01 to 01-03 (3 days) 02-10 to 02-16 (7 days) 02-27 to 03-01 (3 days) 04-02 to 04-05 (4 days) 04-30 to 04-30 (1 day)
Total	73 days

of large trucks heading north from station Yanchao SIC to Tianliao in the southern region. This could be due to the Chinese New Year holidays and the imposition of a restriction on large trucks in that particular area of the southern region.

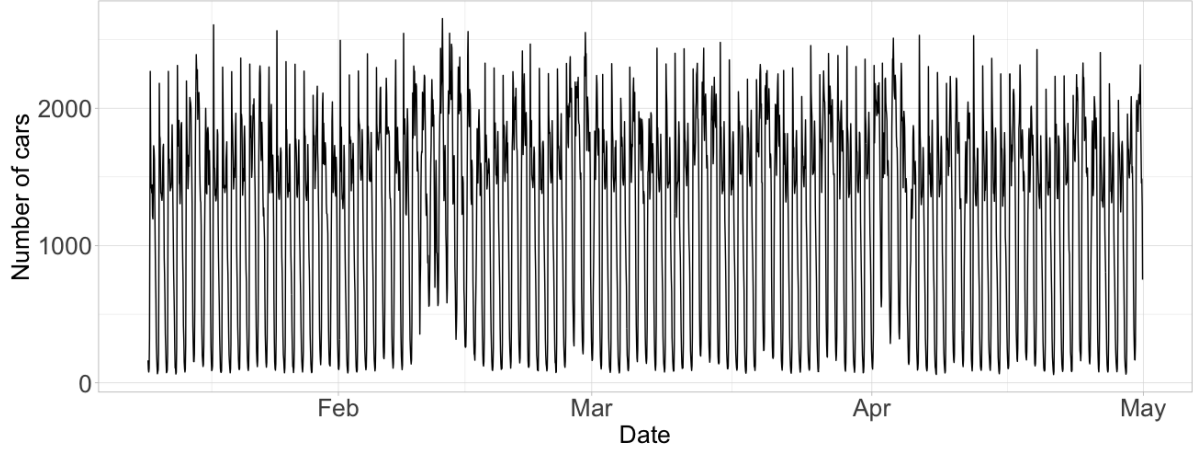
3 Methods

In order to perform anomaly detection in Taiwan traffic time series, we propose to adapt and employ the ordinary least squares (OLS) forecasting model under hierarchy and grouped framework developed by Ashouri et al. (2021). In this paper we refine the OLS model of Ashouri et al. (2021) by incorporating Fourier terms in order to capture the seasonal patterns on a daily and weekly basis in our traffic dataset, while we employ the hierarchy and grouping among traffic time series to embed their spatial correlation and geographical aggregation. In contrast to Ashouri et al. (2021), where the prediction intervals were derived based on the normality assumption, here we construct bootstrap prediction intervals which only require uncorrelated forecast errors. Finally, we employ these intervals for performing prediction-based anomaly detection (Pang et al., 2018) on the Taiwan traffic time series, i.e., we label a point as anomaly if the actual traffic flow value exceeds the prediction interval’s upper bound. The rest of this section details our modeling and anomaly detection framework.

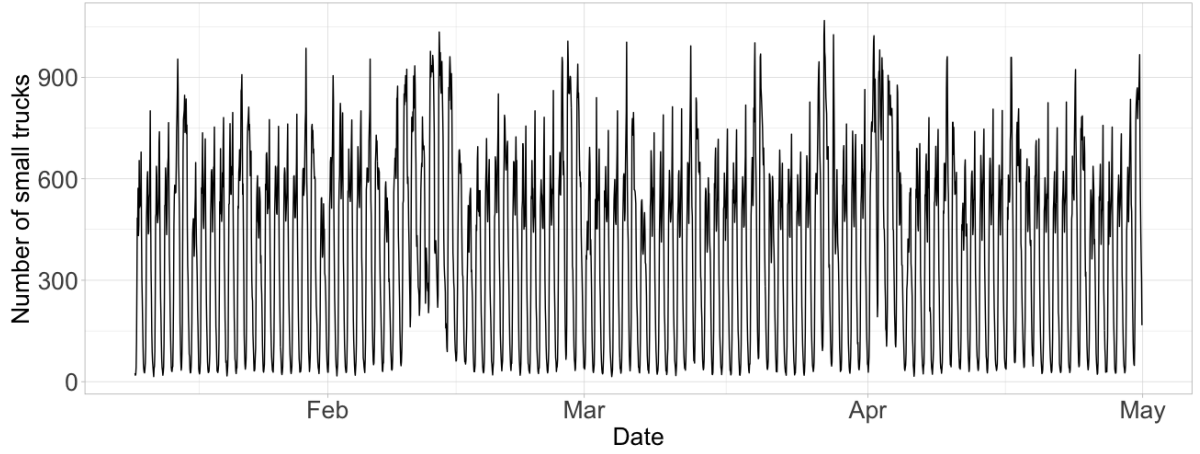
3.1 Hierarchical and grouped time series

In several real-data applications, a large collection of related time series are structured in a hierarchical and/or grouped framework. For instance, traffic data can be disaggregated based on a geographical hierarchy of regions, cities, and stations. Figure 4 shows an example of two-level hierarchy structure. The upper level of the hierarchy (level 0), i.e. the *Total* series, represents the most aggregated time series. At level 1, the *Total* series is disaggregated into series *A* and *B*. Finally, series *A* is disaggregated into series *AA* and *AB*, while *B* into series *BA* and *BB*, at level 2. The most disaggregated level of the hierarchy structure – which is level 2 in the example – is called the bottom-level series. The grouped structure is similar to the hierarchical structure, except that in this case the structure does not disaggregate in a unique hierarchical way (for more details, see Hyndman and Athanasopoulos, 2018).

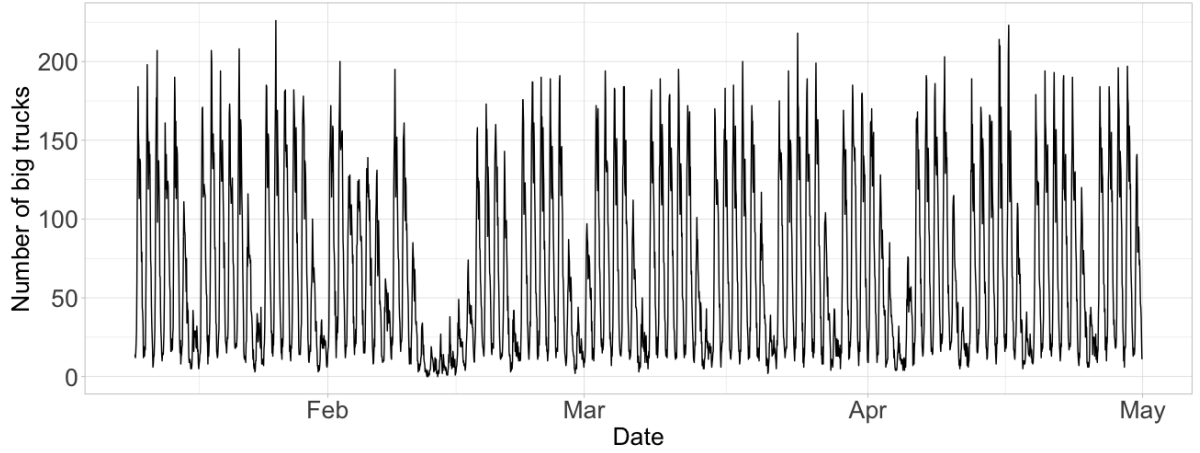
Following the notation in Hyndman and Athanasopoulos (2018), we indicate with y_t the *Total* series for $t = 1, 2, \dots, T$, where T represents the number of time points of the series. For the other series in the



(a) Northern region, Zhongli runway - Hukou, south direction, car



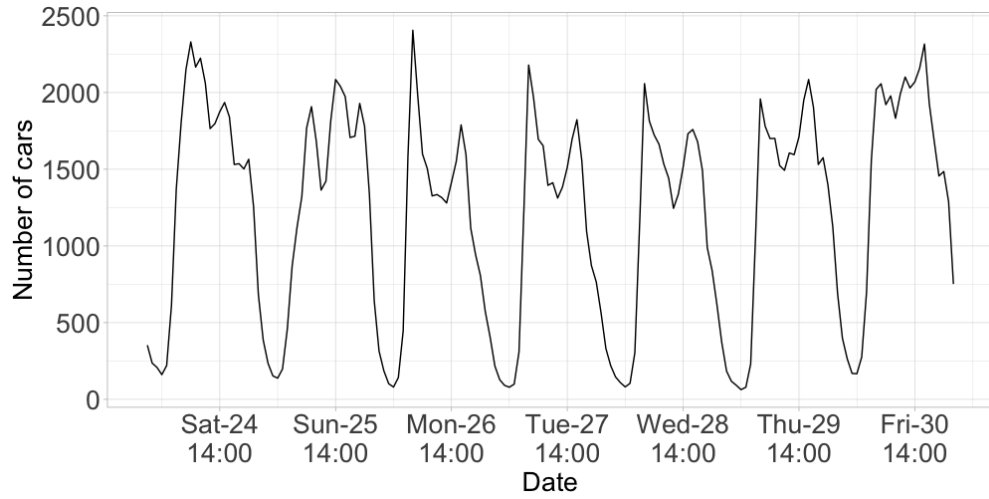
(b) Central region, Xiangshan - Xibin, south direction, small truck



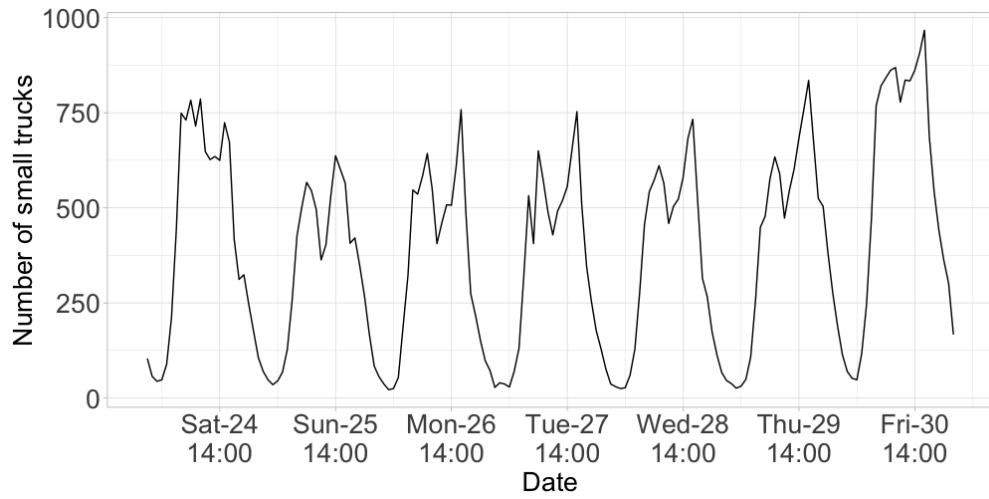
(c) Southern region, Yanchao SIC - Tianliao, north direction, big truck

Figure 2: Examples of Taiwanese highway hourly time series (from 2021-01-10 23:00:00 to 2021-04-30 22:00:00) in three regions for different stations, traffic directions, and vehicle types.

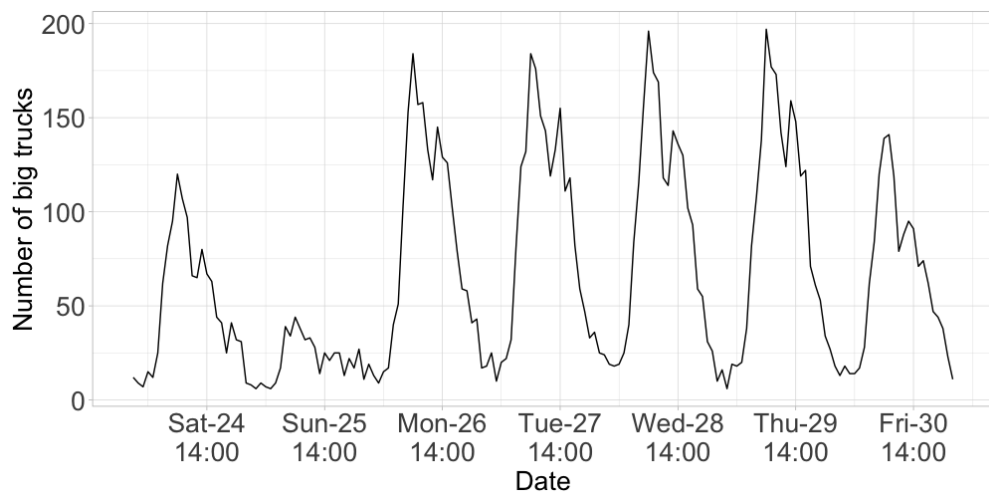
hierarchy structure, y_{jt} represents the t^{th} observation of the series corresponding to node j . For example, in Figure 4, y_{At} and y_{BBt} indicate the t^{th} observation in node A at level 1 and BB at level 2, respectively. In addition, we indicate with \mathbf{S} the *summing matrix*, which represents how bottom-level series are aggregated. Let n be the total number of series in the hierarchy, m the number of bottom-level series, \mathbf{y}_t the n -vector of all the series in the hierarchy, and \mathbf{b}_t the m -vector of all the bottom-level series; the summing matrix \mathbf{S} is the $n \times m$ matrix such that $\mathbf{y}_t = \mathbf{S}\mathbf{b}_t$. For example, the following equation shows the \mathbf{S} matrix for the structure in Figure 4 (in this case, $n = 7$ and $m = 4$):



(a) Northern region, Zhongli runway - Hukou, south direction, car



(b) Central region, Xiangshan - Xibin, south direction, small truck



(c) Southern region, Yanchao SIC - Tianliao, north direction, big truck

Figure 3: Examples of Taiwanese highway hourly time series, zoomed in view on the last seven days of the time series shown in Figure 2 (from 2021-04-23 23:00:00 to 2021-04-30 22:00:00).

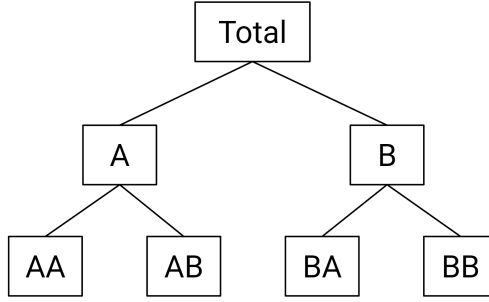


Figure 4: Example of two-level hierarchy structure.

$$\begin{pmatrix} y_t \\ y_{A,t} \\ y_{B,t} \\ y_{AA,t} \\ y_{AB,t} \\ y_{BA,t} \\ y_{BB,t} \end{pmatrix} = \begin{pmatrix} 1 & 1 & 1 & 1 \\ 1 & 1 & 0 & 0 \\ 0 & 0 & 1 & 1 \\ 1 & 0 & 0 & 0 \\ 0 & 1 & 0 & 0 \\ 0 & 0 & 1 & 0 \\ 0 & 0 & 0 & 1 \end{pmatrix} \begin{pmatrix} y_{AA,t} \\ y_{AB,t} \\ y_{BA,t} \\ y_{BB,t} \end{pmatrix}.$$

Importantly, the forecasts in all the hierarchy levels should add up properly. Indeed, if the aggregation constraints are ignored, then the resulting forecasts would not be consistently aggregated and the relationships between the series would be missed (Hyndman and Athanasopoulos, 2018). The methods traditionally used to forecast hierarchical and grouped time series are called single-level approaches and include bottom-up (Kahn, 1998), top-down (Gross and Sohl, 1990), and middle-out (Hyndman et al., 2011) approaches. All these methods select one level of aggregation and generate the forecasts for all series at that level; they then aggregate the forecasts for higher level series and disaggregate them for lower level series. In this paper, we employ a more recent approach called optimal combination which includes two steps. First, the forecasts of all the series in all the levels of aggregation are computed (*base forecasts*); second, the base forecasts are reconciled (*reconciled forecasts*). Let $\hat{\mathbf{y}}_{t+h}$ indicate the h -step-ahead base forecasts; then, the reconciled forecast $\tilde{\mathbf{y}}_{t+h}$ can be computed by the following equation

$$\tilde{\mathbf{y}}_{t+h} = \mathbf{S}(\mathbf{S}'\mathbf{W}_h^{-1}\mathbf{S})^{-1}\mathbf{S}'\mathbf{W}_h^{-1}\hat{\mathbf{y}}_{t+h} = \mathbf{S}\mathbf{G}\hat{\mathbf{y}}_{t+h}, \quad (1)$$

where \mathbf{S} is the summing matrix, $\mathbf{W}_h = \text{Var}(\mathbf{y}_{t+h} - \hat{\mathbf{y}}_h)$, and $\mathbf{S}\mathbf{G}$ is the *reconciliation matrix*. Since estimating \mathbf{W}_h from data is generally challenging, some approximations have been proposed in the literature. In this paper, we apply the *shrinkage estimator* (Wickramasuriya et al., 2019), which shrinks the full covariance matrix (of the errors on one-step predictions made on the training data) toward a diagonal matrix⁵.

In our Taiwan traffic dataset, the hierarchy and grouped structure is defined by geographic divisions, highway number, direction, and type of vehicle. In particular, a first geographic division is represented by the three network regions, i.e., “north”, “center”, and “south”. The second level in the hierarchical structure divides the dataset into 319 stations (see Figure 1). In addition, the data has a grouped structure with the three following attributes:

1. Highway number: no.1, elevated no.1, and no.3;
2. Highway direction: north, south, east, and west;
3. Vehicle type: car, small truck, bus/coach, big truck, and tractor-trailer.

This structure results in a total of 1998 series, when considering all levels. Table 2 displays all the aggregation levels and the combinations applied in the reconciliation step (see Subsection 3.2), with the number of series at each hierarchy level. Note that, for simplicity, we only include two-way combinations in the reconciliation step. Including also three-way combinations could slightly improve the results.

⁵The *shrinkage estimator* is given by:

$$\mathbf{W}_h = k_h \hat{\mathbf{W}}_{1D}^*,$$

$$\hat{\mathbf{W}}_{1D}^* = \lambda_D \hat{\mathbf{W}}_{1D} + (1 - \lambda_D) \hat{\mathbf{W}}_1,$$

where $\hat{\mathbf{W}}_{1D}$ is a diagonal matrix comprising only the diagonal entries, $\hat{\mathbf{W}}_1 = \frac{1}{T} \sum_{t=1}^T \hat{\mathbf{e}}(\mathbf{1})_t \hat{\mathbf{e}}(\mathbf{1})_t'$ is the unbiased sample covariance estimator of the in-sample one-step-ahead base forecast errors,

$$\hat{\lambda}_D = \frac{\sum_{i \neq j} \widehat{\text{Var}}(\hat{r}_{ij})}{\sum_{i \neq j} \hat{r}_{ij}^2},$$

and \hat{r}_{ij} is the ij^{th} element of the 1-step-ahead sample correlation matrix (Wickramasuriya et al., 2019).

Table 2: Number of highway traffic series at each aggregation level.

Aggregation level	Series
Taiwan	1
Region	3
Station	319
Highway	3
Direction	4
Vehicle type	5
Region x Direction	8
Region x Highway	7
Region x Vehicle type	15
Highway x Direction	8
Highway x Vehicle type	15
Direction x Vehicle type	20
Bottom-level series	1590
Total	1998

Other fundamental features of our traffic data which must be included in the model are the complex seasonal patterns (daily and weekly seasonality), the autocorrelation, and the spatial correlations (traffic volumes at nearby locations are highly correlated; Li et al., 2019b). The OLS approach we propose includes specific terms to handle autocorrelation and multiple seasonalities (see Subsection 3.2), while spatial correlation is already embedded in the hierarchical structure of the series and is taken care of in the reconciliation step (Wickramasuriya et al., 2019). For previous research on traffic forecast, we refer to Li et al. (2019b), who combined the gradient boosting procedure with hierarchical reconciliation for short-term traffic flow forecasting. In contrast to the approach proposed in Li et al. (2019b), which involves a complex method that may encounter computation difficulties, our approach employs a straightforward and interpretable linear model that performs effectively on intricate highway problems.

3.2 Ordinary least squares forecast reconciliation

To calculate the base forecasts (\hat{y}_{t+h}), we employ OLS models with relevant predictors for forecasting hourly traffic time series. While being very simple and computationally efficient, OLS models can provide very good approximations of more complex models’ forecasts (Ashouri et al., 2018, 2019). Moreover, the computational benefits of OLS approach allows us to use bootstrap to compute the prediction intervals, avoiding specific distribution assumptions. Our predictor set includes linear trend, seasonality, and lag variables. In particular, we assume daily and weekly seasonality, hence we include Fourier terms (Hyndman and Athanasopoulos, 2018) for each of these two seasonal periods (periods of 24 and $7 \times 24 = 168$ hours for daily and weekly seasonality, respectively). To capture time series autocorrelation, we include the first and the 24th lags among our predictors (see Appendix A for details on the selection of terms for the OLS model). Hence, the proposed OLS model is

$$\begin{aligned}
 y_t = & \alpha_0 + \alpha_1 t + \sum_{k_1=1}^{l_1} \beta_{k_1} \sin\left(\frac{2\pi k_1 t}{24}\right) + \sum_{k_1=1}^{l_1} \beta'_{k_1} \cos\left(\frac{2\pi k_1 t}{24}\right) \\
 & + \sum_{k_2=1}^{l_2} \gamma_{k_2} \sin\left(\frac{2\pi k_2 t}{7 \times 24}\right) + \sum_{k_2=1}^{l_2} \gamma'_{k_2} \cos\left(\frac{2\pi k_2 t}{7 \times 24}\right) \\
 & + \eta_1 y_{t-1} + \eta_{24} y_{t-24} + \varepsilon_t,
 \end{aligned} \tag{2}$$

where y_{t-k} is the k^{th} lagged value for y_t , $l_1 = 3$, $l_2 = 2$, and ε_t is the error term. For computing base forecasts, one OLS model with the same set of predictors in Equation 2 is fitted to every single series in the hierarchical and grouped structure. The forecast is then reconciled by using Equation 1. Algorithm 1 shows the procedure we propose for calculating base and reconciled forecasts.

To forecast traffic flow and evaluate the performance of our approach on Taiwan traffic data (see Subsection 4.1), we employ a blocked cross-validation approach. This approach uses a sliding window of a fixed size for selecting training and test data within a time series, respecting the order of the values in the time series. In particular, the first cross-validation split considers the starting T_{train} time points of the series as a training set and the next T_{test} time points as a test set. Then, the test set time points are added to the training set, while an equal amount of points are removed from the beginning of the training set; the new

Algorithm 1 Computing base and reconciled forecasts using OLS models

```

1: Forecast horizon :  $h$ 
2: for  $i \in \{1, \dots, N\}$  do
3:   Time series :  $\mathbf{y}_i = (y_{1,i}, y_{2,i}, \dots, y_{T,i})$ 
4:    $P$  predictors:  $\mathbf{X}_i = \{(x_{1,i,1}, x_{2,i,1}, \dots, x_{T,i,1}), \dots, (x_{1,i,p}, x_{2,i,p}, \dots, x_{T,i,p})\}$ 
5:   Model:  $fit = lm(y_{t,i} \sim x_{t,i,1} + x_{t,i,2} + \dots + x_{t,i,p}, data = (\mathbf{y}_i, \mathbf{X}_i))$ 
6:    $P$  new predictors:  $\mathbf{X}_i^\dagger = \{(x_{T+1,i,1}, x_{T+2,i,1}, \dots, x_{T+h,i,1}), \dots, (x_{T+1,i,p}, x_{T+2,i,p}, \dots, x_{T+h,i,p})\}$ 
7:   for  $j \in \{1, \dots, h\}$  do
8:     Prediction:  $\hat{y}_{t+j,i} = predict(fit, newdata = \mathbf{X}_{t+j,i}^\dagger)$ 
9:   end for
10: end for
11: Reconcile forecasts:  $\tilde{\mathbf{y}} = \mathbf{S}\mathbf{G}\hat{\mathbf{y}}$ 

```

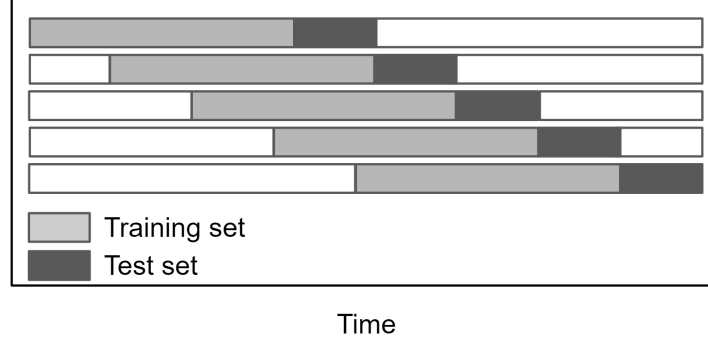


Figure 5: Blocked cross-validation approach for computing forecasts in Taiwan's traffic flow time series.

test set is constituted by the next T_{test} time points. The procedure is repeated until the test set reaches the end of the time series. Figure 5 displays this procedure for creating training (light gray) and test (dark gray) sets. Importantly, this approach allows us to compute the forecasts for the whole series (except the first T_{train} time points).

3.3 Bootstrapped prediction intervals

Bootstrapped prediction intervals are useful when the normality assumption for the error term is unreasonable, and we can only assume uncorrelated forecast errors with constant variance. In this paper, we forecast the count of vehicles per hour, hence it is advisable to drop the assumption of normality and apply the bootstrap approach⁶. For this reason, we propose the Algorithm 2 to compute the bootstrapped reconciled prediction interval for our traffic data.

The proposed approach starts by estimating the OLS coefficients and computing the residuals e_j for $j = 1, 2, \dots, T$ for each series. Then, these residuals are modified as $\{s_1 - \bar{s}, s_2 - \bar{s}, \dots, s_T - \bar{s}\}$ where \bar{s} is s_j 's average for $j = 1, 2, \dots, T$ and

$$s_j = \frac{e_j}{\sqrt{1 - h_j}}, \quad (3)$$

with h_j the leverage of the j^{th} observation. Note that these *modified residuals* are employed in order to adjust the residuals' variance differences and make their variance constant (Davison and Hinkley, 1997). In the next step, a bootstrap sample is randomly drawn from the modified residuals for each forecast point and it is added to the forecast (sample path). This step is repeated K times, where K represents the number of bootstrap samples. Finally, the reconciled prediction interval is computed by reconciling the sample paths and then calculating the required percentiles (see steps 17 and 18 in Algorithm 2; Hyndman and Athanasopoulos, 2018).

4 Results

We present the results of two analyses of Taiwan traffic data. First, we model and forecast four months of Taiwanese highway time series (from 2021-01-01 to 2021-04-30) using the OLS forecasting model under the hierarchy and grouped structure proposed in Subections 3.1 and 3.2, and we compare the results to the

⁶ibarraespinoza.github.io/VEINBOOK/traffic.html

Algorithm 2 Computing bootstrapped reconciled prediction intervals

```
1: Number of series:  $N$ 
2: Length of each series:  $T$ 
3: Forecast horizon :  $h$ 
4: Number of bootstrap samples:  $K$ 
5: for  $i \in \{1, \dots, N\}$  do
6:   Base forecast model:  $\mathbf{y}_i = \mathbf{X}_i \mathbf{B} + \epsilon_i$ 
7:   Estimate the coefficients:  $\hat{\mathbf{B}} = (\mathbf{X}_i' \mathbf{X}_i)^{-1} \mathbf{X}_i' \mathbf{y}_i$ 
8:   Modified residuals:  $\mathbf{s} = \{s_1 - \bar{s}, s_2 - \bar{s}, \dots, s_T - \bar{s}\}$  from model's residuals  $\mathbf{e} = \{e_1, e_2, \dots, e_T\}$ 
9:   for  $j \in \{1, \dots, h\}$  do
10:    Compute forecasts:  $\hat{\mathbf{y}}_{ij} = \mathbf{X}_{ij}^\dagger \hat{\mathbf{B}}$ 
11:    for  $k \in \{1, \dots, K\}$  do
12:      Draw one sample from  $\mathbf{s}$ :  $\mathbf{s}_k^*$ 
13:      Generate future values for  $i^{\text{th}}$  time series ( $k^{\text{th}}$  sample path):  $\hat{\mathbf{y}}_{ij}^{[k]} = \mathbf{X}_{ij}^\dagger \hat{\mathbf{B}}^* + \mathbf{s}_k^*$ 
14:    end for
15:  end for
16: end for
17: Reconcile the sample paths:  $(\mathbf{SG}\hat{\mathbf{y}}^{[1]}, \mathbf{SG}\hat{\mathbf{y}}^{[2]}, \dots, \mathbf{SG}\hat{\mathbf{y}}^{[K]})$ 
18: Compute pointwise  $\frac{\alpha}{2}$  and  $1 - \frac{\alpha}{2}$  percentiles from reconciled sample paths:  $p_t^{\frac{\alpha}{2}}$  and  $p_t^{1-\frac{\alpha}{2}}$ 
19:  $(1 - \alpha)\%$  bootstrapped prediction interval:  $(p_t^{\frac{\alpha}{2}}, p_t^{1-\frac{\alpha}{2}})$ 
```

ones obtained with Autoregressive Integrated Moving Average (ARIMA) model. This analysis allows us to evaluate the performance of the proposed OLS model prior to its application in detecting traffic anomalies in consecutive holidays. Second, we focus on the 73 days of consecutive holidays of Table 1 and we perform anomaly detection using the method presented in Subsections 3.2 and 3.3.

4.1 Forecasting highway traffic flow

We consider Taiwan's hourly traffic data from 2021-01-01 to 2021-04-30, and we model them using the proposed OLS approach in order to evaluate the forecast performance of this simple and computationally efficient model and to compare it to the forecasting results obtained by ARIMA model. We considered another suitable method, the Exponential smoothing state space model with Box-Cox transformation (TBATS; Hyndman and Athanasopoulos, 2018). However, we dropped it because it is too computationally expensive to be employed on our traffic dataset. The ARIMA model is fitted using the function `auto.arima` from the R package `forecast` (Hyndman and Khandakar, 2008), with default options, while for the OLS model, we employ the `lm` function from the `stats` R package. Note that `auto.arima` function automatically selects the best ARIMA model for each time series according to AICc, while OLS model is fixed (see Subsection 3.2). For both approaches, we include the same Fourier terms for the two seasonal periods (daily and weekly seasonalities, see Subsection 3.2), as well as the same hierarchical and group structure. Following the blocked cross-validation approach (Subsection 3.2), we partition the data into 106 training and test set pairs, comprising 336 hours (T_{train} ; two weeks) and 24 hours (T_{test} , one day), respectively. Prediction intervals are generated based on 2000 bootstrap samples.

Figure 6 shows the comparison of the forecast error distributions for ARIMA and OLS approaches, for all the aggregation levels, while Table 3 reports the average Root Mean Square Errors (RMSEs) and its standard error across all the series in each aggregation level. Note that the errors are larger in magnitude for higher count series (i.e., higher aggregation levels). We observe that the two methods behave similarly, without substantial bias in all aggregation levels. Interestingly, OLS model behave better than ARIMA model, on average, in about half of the aggregation level, despite being much simpler and despite the fact that the best ARIMA model is automatically selected for each time series.

Figure 7 compares the OLS and ARIMA approaches' forecast results and prediction intervals for the three bottom-level series of Figures 2-3, as well as for the Taiwan total series, in 7 days (from 2021-04-24 to 2021-04-30). We observe that the forecast results from the two methods are similar in all four series and days, except for the most variable lower count series of Figure 7d in 2021-04-25. One possible explanation for the fact that the sudden decrease in the number of big trucks traveling on Sundays along this particular highway cannot be forecasted by OLS model, is that it may mainly rely on the previous day pattern, while ARIMA might better capture the pattern that may have occurred during Sundays of previous weeks. In terms of prediction intervals, ARIMA's intervals are generally larger than OLS' ones, especially for the lower count series. Note that the last day depicted in Figure 7 (2021-04-30) is the first day of a consecutive holiday, and in the first three series (Figures 7a, 7b, and 7c), the actual traffic flow is higher than the

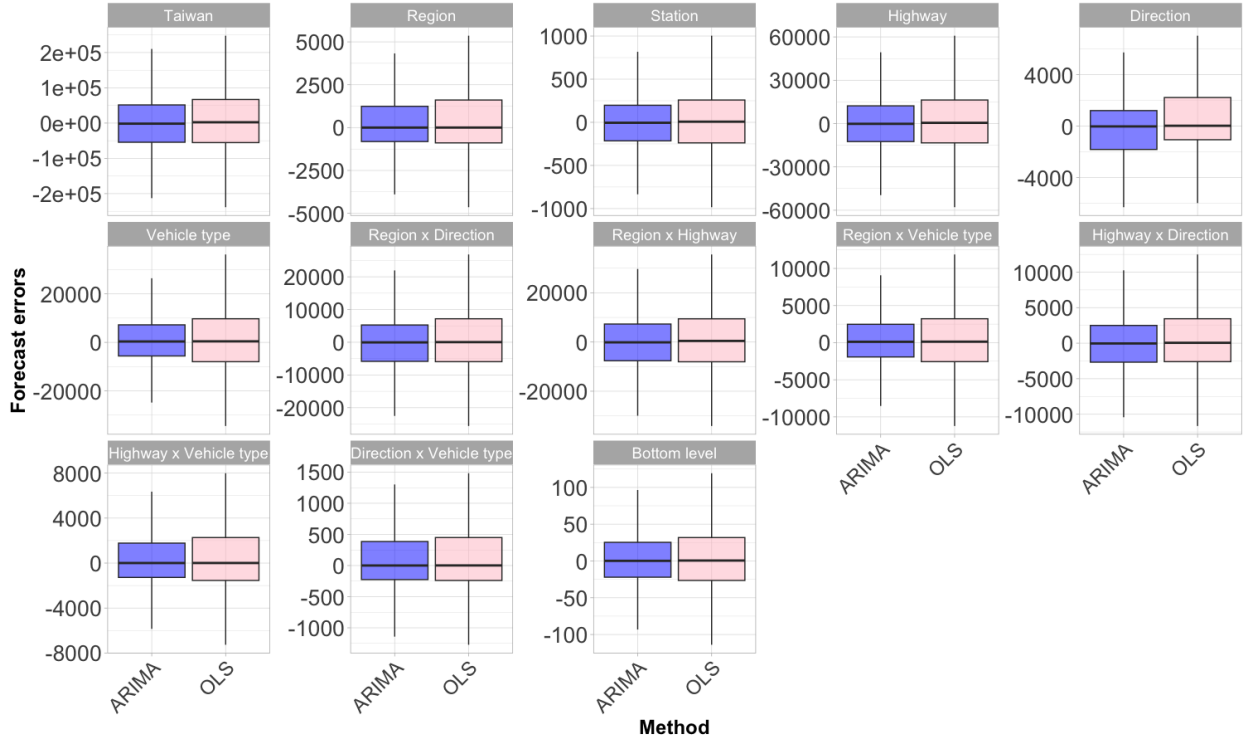


Figure 6: Boxplots of forecast errors from ARIMA and OLS methods at each aggregation level.

Table 3: Average and standard error (in parenthesis) of RMSE on test sets for ARIMA and OLS. Cells corresponding to the best average RMSE are highlighted in gray.

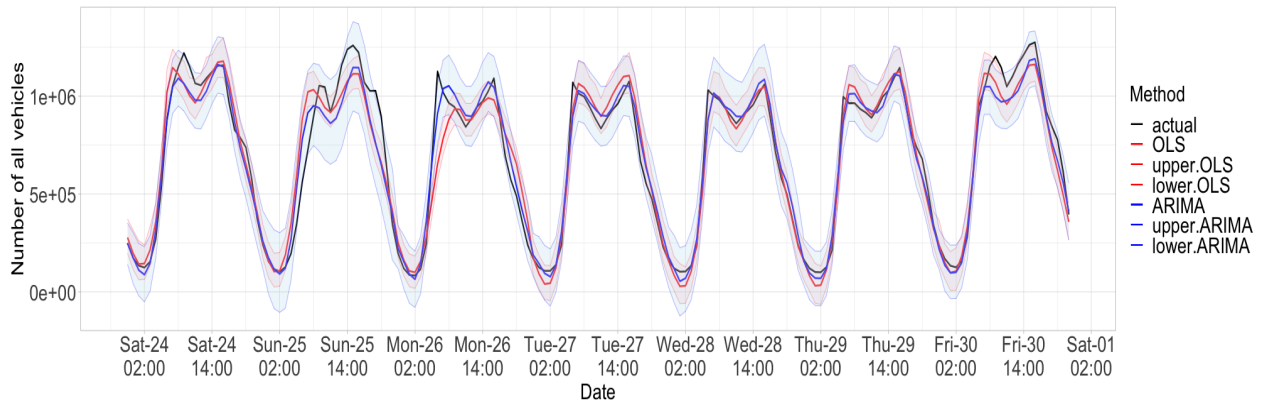
Aggregation level	ARIMA	OLS
Taiwan	107038 (2120)	115232 (2279)
Region	22432 (72)	21533 (69)
Station	534 (0.59)	546 (0.60)
Highway	45211 (517)	46911 (536)
Direction	41272 (409)	43070 (426)
Vehicle type	51083 (453)	48236 (427)
Region x Direction	19975 (140)	20175 (141)
Region x Highway	20122 (151)	20221 (151)
Region x Vehicle type	18918 (67)	17699 (91)
Highway x Direction	21405 (150)	21722 (152)
Highway x Vehicle type	20851 (107)	19414 (99)
Direction x Vehicle type	19104 (85)	17854 (79)
Bottom-level series	221 (0.11)	214 (0.11)

Table 4: Computation time (seconds) for ARIMA and OLS with reconciliation, for one cross-validation split.

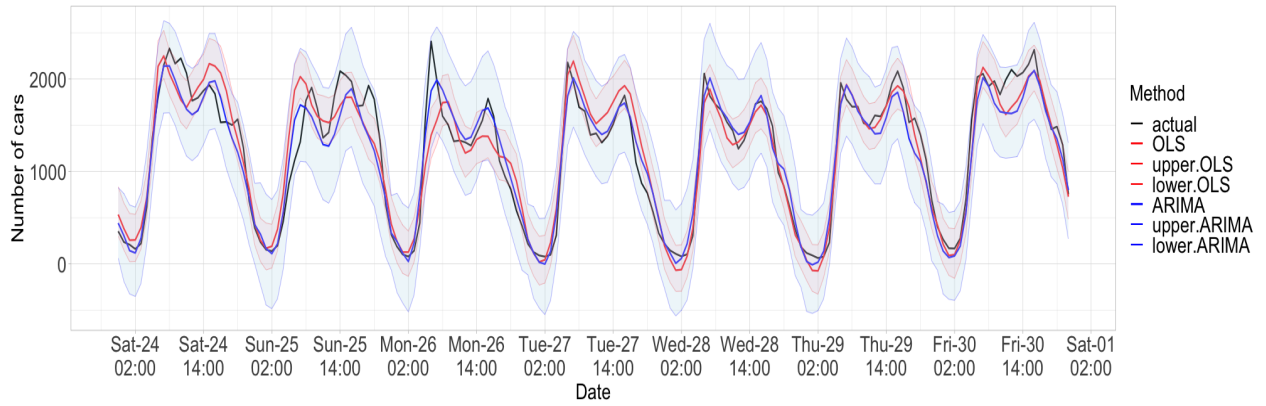
	ARIMA	OLS
Base forecast	3164	578
Reconciling forecasts	26	26
Reconciling sample paths	894	894

forecasted values for both methods. In particular, both models detect anomalies in Figure 7c, where they under-forecast the actual series. The big truck series (Figure 7d) shows a different pattern, in which the observed count is actually lower than the forecasted one in both OLS and ARIMA approaches.

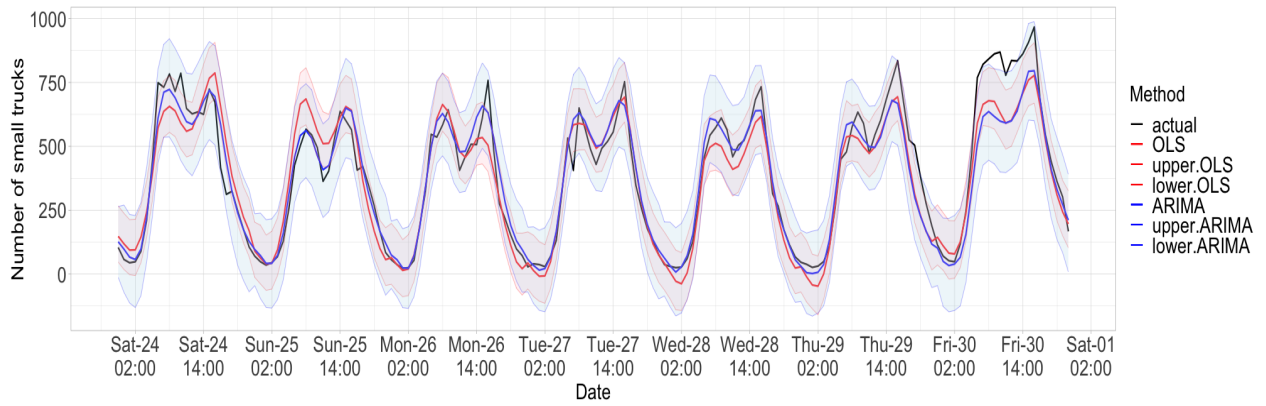
Finally, Table 4 compares the computation time of the two approaches, including base forecast, forecast reconciliation, and sample paths (2000 bootstrap samples) reconciliation steps. Note that we forecast each day independently, and this computation time refers to the forecast for one day (one split of the blocked



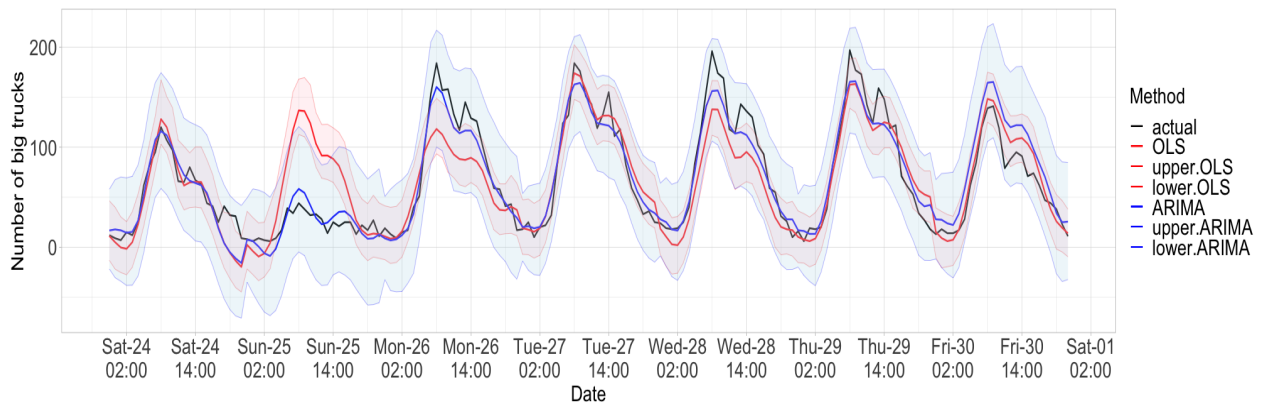
(a) Taiwan



(b) Northern region, Zhongli runway - Hukou, south direction, car



(c) Central region, Xiangshan - Xibin, south direction, small truck



(d) Southern region, Yanchao SIC - Tianliao, north direction, big truck

Figure 7: OLS and ARIMA forecasting with bootstrapped prediction intervals for Taiwan series as well as for the three bottom-level series of Figures 2-3 (7 days, from 2021-04-24 to 2021-04-30).

cross-validation). The two methods are run on a Linux server (Compute Canada: docs.alliancecan.ca/wiki/Technical_documentation) using R version 4.2.1. Compared to the ARIMA approach, the OLS model is much faster in the base forecast step, despite having similar forecasting performance.

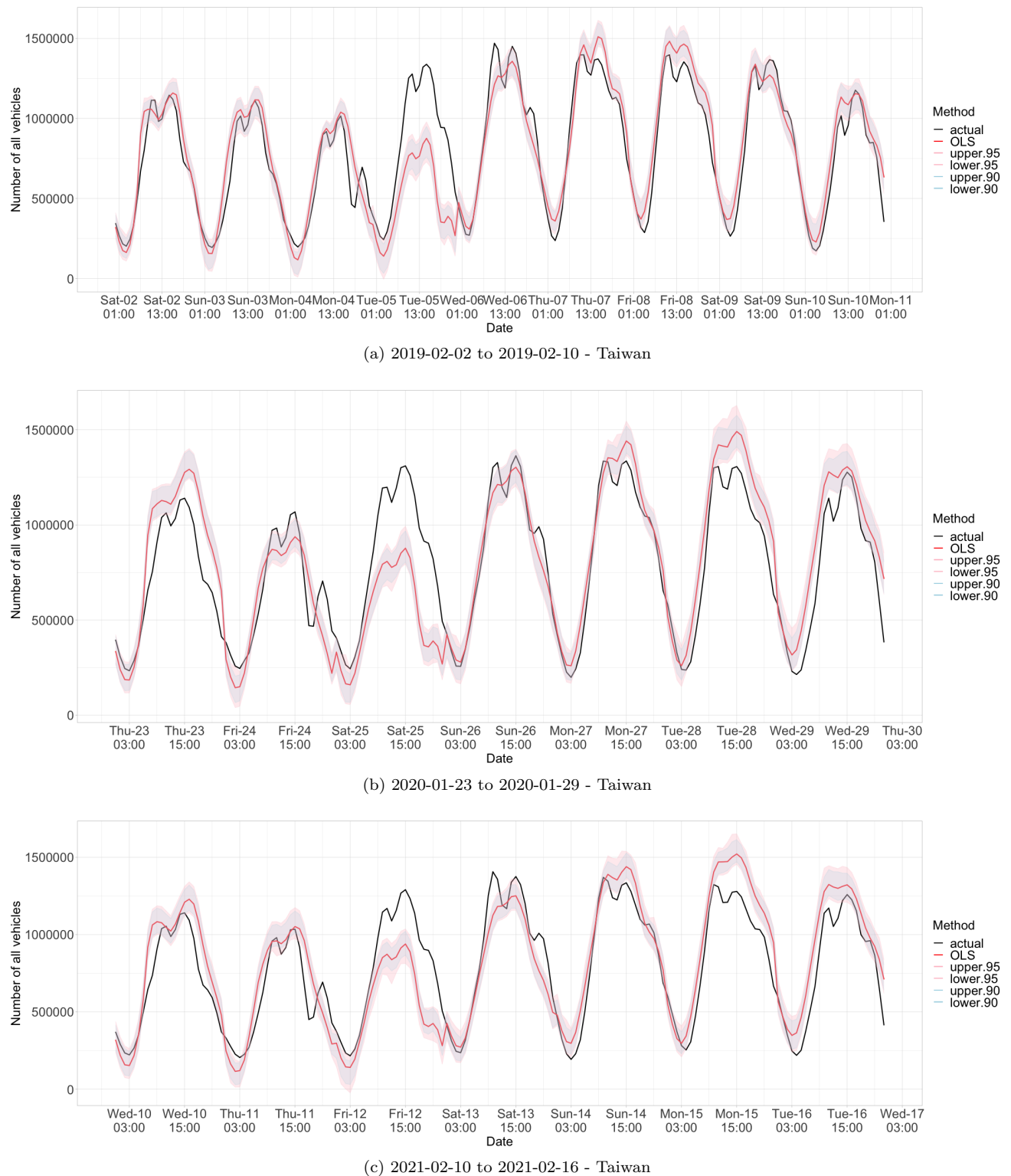
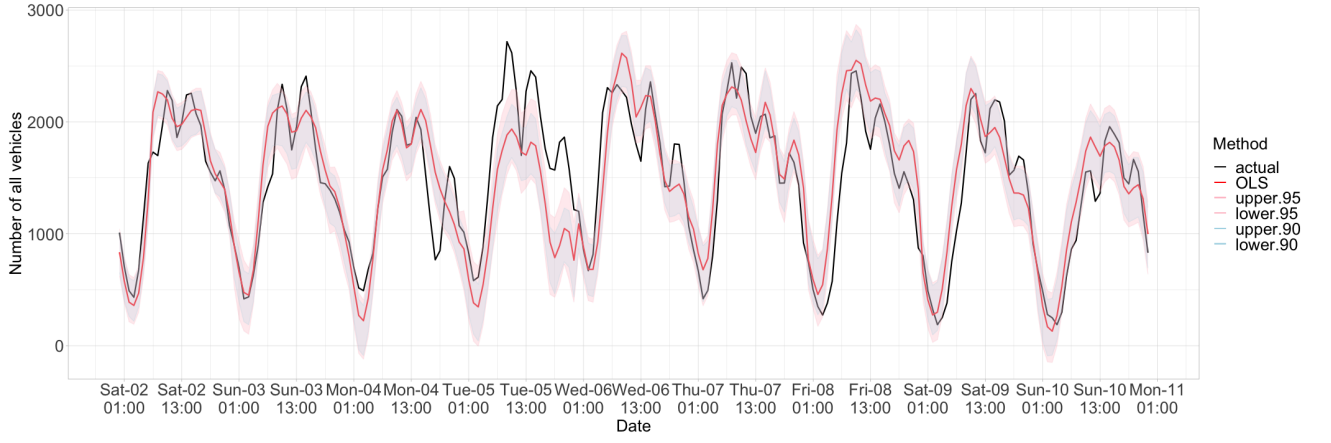
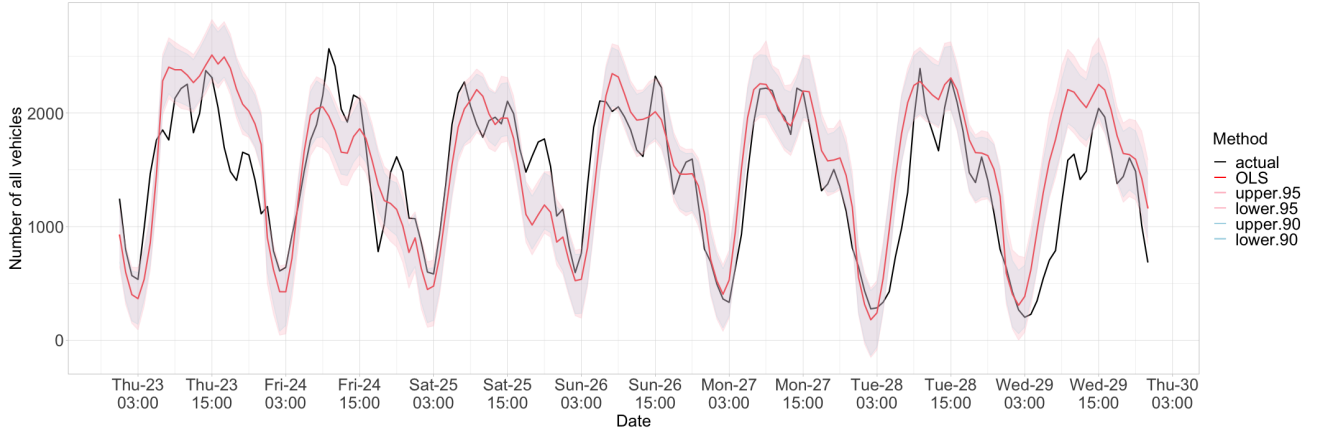


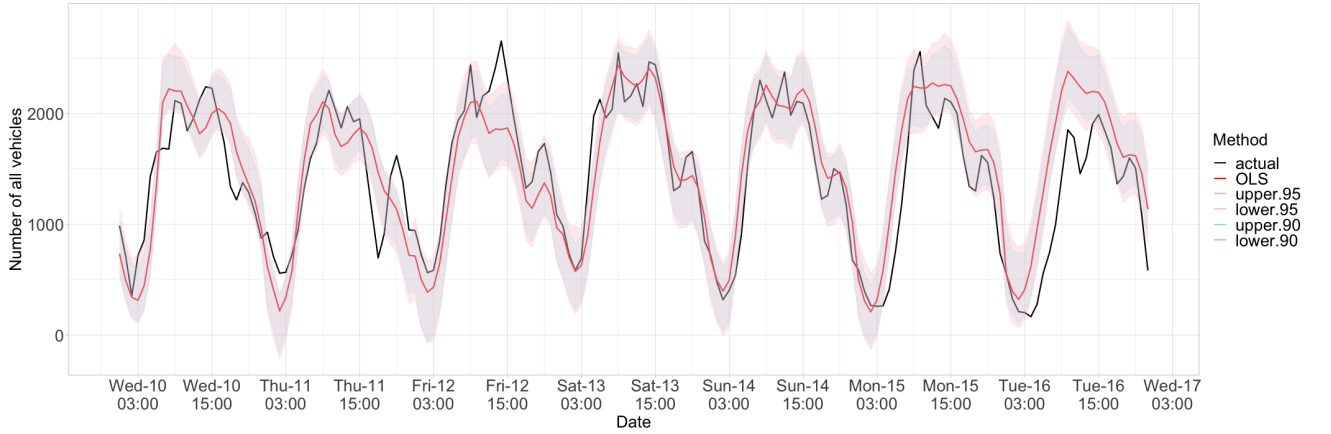
Figure 8: OLS forecasting with its 90% and 95% bootstrapped prediction intervals for Taiwan series in three consecutive long holidays – 2019-02-02 to 2019-02-10, 2020-01-23 to 2020-01-29, and 2021-02-10 to 2021-02-16.



(a) 2019-02-02 to 2019-02-10 - Northern region, Zhongli runway - Hukou, south direction, car



(b) 2020-01-23 to 2020-01-29 - Northern region, Zhongli runway - Hukou, south direction, car



(c) 2021-02-10 to 2021-02-16 - Northern region, Zhongli runway - Hukou, south direction, car

Figure 9: OLS forecasting with its 90% and 95% bootstrapped prediction intervals for the bottom-level series of Figures 2a and 3a in three consecutive long holidays – 2019-02-02 to 2019-02-10, 2020-01-23 to 2020-01-29, and 2021-02-10 to 2021-02-16.

4.2 Consecutive holidays anomaly detection

We study the 73 days which are part of 18 consecutive holidays in 2019, 2020, and 2021 (see Table 1), modeling them using the proposed OLS approach, taking 5000 bootstrap samples to generate prediction intervals. In order to forecast the traffic in each 24-hour period (T_{test} ; one day) during consecutive holidays, we train the model on the data from the preceding 336 hours (T_{train} ; two weeks).

Figures 8 and 9 display the OLS forecasting as well as its 90% and 95% bootstrapped prediction intervals, for Taiwan total series and for the bottom-level series of Figures 2a and 3a, in the three longest consecutive holidays, i.e. 2019-02-02 to 2019-02-10, 2020-01-23 to 2020-01-29, and 2021-02-10 to 2021-02-16. Figure 8

Table 5: Number of detected anomalies per day (divided by holiday length) in the 18 long holidays in the northern, central, and southern regions in the north, south, east, and west directions, divided into four time intervals: 00:00-05:00 (1), 06:00-11:00 (2), 12:00-17:00 (3), and 18:00-23:00 (4). Cell background colors are proportional to the number of anomalies per day (white for 0-1.5 anomalies, light gray for 1.5-3 anomalies, gray for 3-4.5 anomalies, and dark gray for 4.5 or more anomalies).

Holiday	North direction												South direction												East direction				West direction																																																																																																																																																																																																																																																																																																																																																																																																																																																																																																																																																																																																																																																																																																																																																																																																																																																																																																																																																																																																																																																																																																																																																																																																																																																																																																																																																																																																																																																																																																																																																																																																																																																																																						
	North				Center				South				North				Center				South				North				Center				East direction				West direction																																																																																																																																																																																																																																																																																																																																																																																																																																																																																																																																																																																																																																																																																																																																																																																																																																																																																																																																																																																																																																																																																																																																																																																																																																																																																																																																																																																																																																																																																																																																																																																																																																																																														
	1	2	3	4	1	2	3	4	1	2	3	4	1	2	3	4	1	2	3	4	1	2	3	4	1	2	3	4	1	2	3	4	1	2	3	4	1	2	3	4																																																																																																																																																																																																																																																																																																																																																																																																																																																																																																																																																																																																																																																																																																																																																																																																																																																																																																																																																																																																																																																																																																																																																																																																																																																																																																																																																																																																																																																																																																																																																																																																																																																																											
2019																																																																																																																																																																																																																																																																																																																																																																																																																																																																																																																																																																																																																																																																																																																																																																																																																																																																																																																																																																																																																																																																																																																																																																																																																																																																																																																																																																																																																																																																																																																																																																																																																																																																																																																			

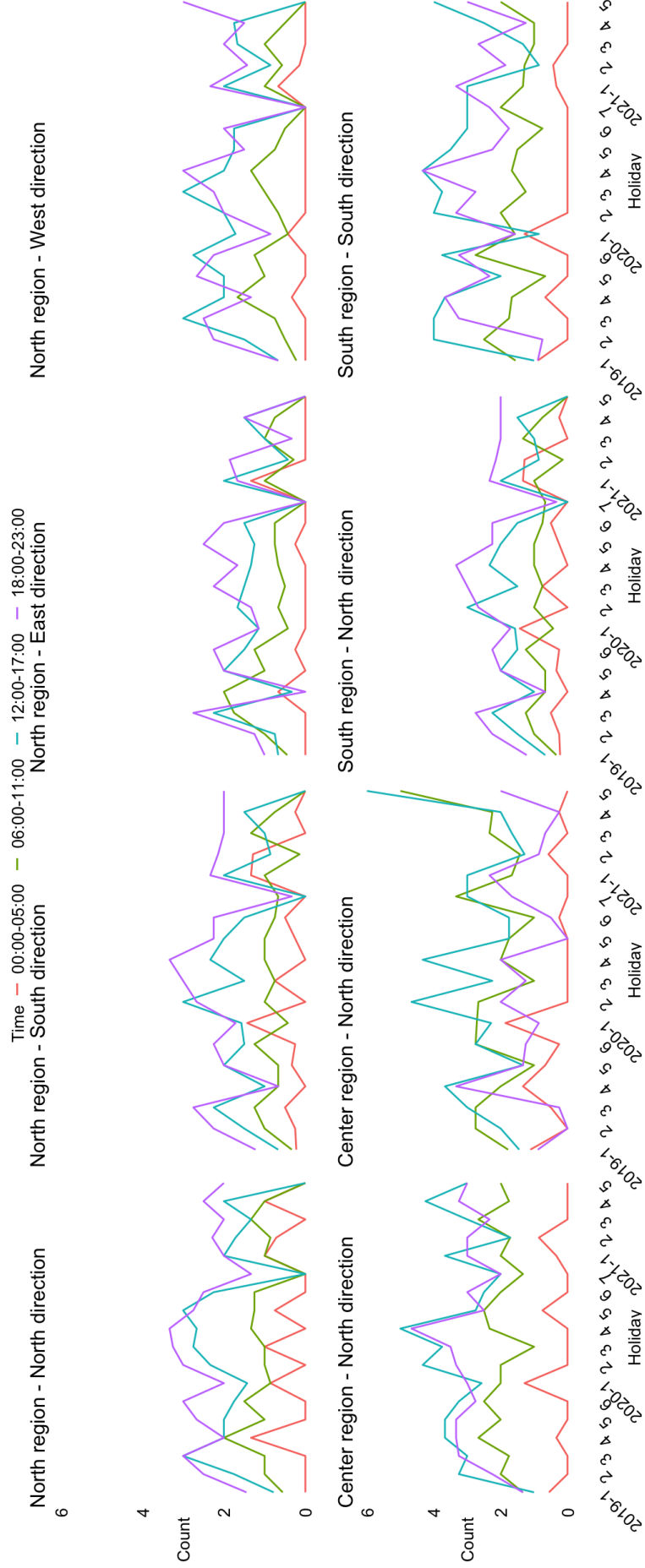


Figure 10: Number of detected anomalies per day (divided by holiday length) in the 18 long holidays in the northern, central, and southern regions in the north, south, east, and west directions, divided in four time intervals: 00:00-05:00 (1), 06:00-11:00 (2), 12:00-17:00 (3), and 18:00-23:00 (4).

illustrates traffic flow in Taiwan (total series) during the Lunar New Year holidays, highlighting unexpected spikes (anomalies) on the first day of the Chinese New Year (2019-02-05, 2020-01-25, and 2021-02-12). These two figures also show that the prediction intervals at 90% and 95% are pretty similar and anomaly detection is not very sensitive to changing the prediction level from 90% to 95%; thus, we focus on the 95% prediction intervals in the following results.

Table 5 reports the number of detected anomalies per day (divided by holiday length) in each of the three regions and in each direction. In this table, the day is divided into four time intervals, i.e. 00:00 to 05:00, 06:00 to 11:00, 12:00 to 17:00, and 18:00 to 23:00. The same results are also displayed in Figure 10. Additional anomaly detection results based on the highway direction and number are presented in Table 7 and Figure 13. In general, we detect a small number of anomalies during the night (from 00:00 to 05:00), especially in the east and west directions. In the north direction, anomalies are mostly in the center and south regions, in the afternoon and evening (from 12:00 to 23:00), while in the south direction, anomalies are typically detected in the center region, in the morning and afternoon (from 6:00 to 17:00) and in the south region during afternoon and evening hours (from 12:00 to 23:00). Highways No.1 and No.3 have more anomalies in both north and south directions, with No.3 exhibiting a higher anomaly frequency than No.1 on both highways. Anomalies on highway No.1 in the north direction are more frequent in the evening hours (from 18:00 to 23:00), while on highway No.3, anomalies occur more frequently in the afternoon and evening (from 12:00 to 23:00). In the south direction, the No.1 highway exhibits more anomalies from 12:00 to 23:00, while the No.3 highway has a higher anomaly frequency from 12:00 to 18:00. In the west direction in the elevated No.1 highway, there are similar portions of anomalies during afternoons and evenings (from 12:00 to 17:00 and from 18:00 to 23:00). Interestingly, the number of anomalies has remained relatively stable from 2019 to 2021, with no discernible upward or downward trend (Figure 10).

Finally, Table 6 summarizes the most frequent traffic flow anomalies in Taiwan’s consecutive holidays in 2019, 2020, and 2021. We observe that in the north direction, anomalies are mainly in the central and southern areas of highways No.1 and No.3 during afternoons and evenings (from 12:00 to 23:00). In the south direction, most traffic flow anomalies are in the southern region of highway No.3 during the afternoon and evening (from 12:00 to 17:00) in 2019 and 2020, while in 2021, anomalies are mostly in the central area during the morning hours (from 6:00 to 17:00). The elevated No.1 highway is the only highway that includes the east and west directions (in the northern region). In this highway, anomalies in the east direction are mostly during the evening (from 18:00 to 23:00), while in the west direction anomalies are mostly detected during the afternoon and evening (from 12:00 to 23:00).

Table 6: Summary of the most frequent anomalies on consecutive holidays by direction, region, highway, and time interval in 2019, 2020, and 2021.

Year		North direction	South direction	East direction	West direction
2019	Region	Center/South	South	North	North
	Highway	No.1/No.3	No.3	Elevated No.1	Elevated No.1
	Time	12:00-23:00	12:00-23:00	18:00-23:00	12:00-23:00
2020	Region	Center/South	South	North	North
	Highway	No.1/No.3	No.3	Elevated No.1	Elevated No.1
	Time	12:00-23:00	12:00-17:00	18:00-23:00	12:00-23:00
2021	Region	Center/South	Center	North	North
	Highway	No.1/No.3	No.3	Elevated No.1	Elevated No.1
	Time	12:00-23:00	6:00-17:00	18:00-23:00	12:00-23:00

5 Conclusion

In this study, we explored the Taiwanese highway hourly traffic data with the main objectif of detecting anomalies during long holidays (e.g., Chinese New Year). Understanding where and when most anomalies occur is of utmost importance to help the Taiwanese government and the national freeway bureau evaluating and adjusting their traffic control policies. Our results suggest that based on the highway direction, north and south directions show more anomalies in highway No.3 in the afternoon and central and southern Taiwan for the north direction and southern Taiwan for the south direction. East and west directions included fewer anomalies, which were mainly in the 12:00-23:00 period.

To perform this traffic anomaly detection, we employed a fast OLS approach which allows to efficiently model the complex hourly traffic dataset with reasonable accuracy, and bootstrapped prediction intervals which relies only on the assumption of uncorrelated forecast errors. The proposed model captures traffic

seasonality and spatial correlation using Fourier terms and hierarchical aggregation. While other more complex models like ARIMA require high computation time for forecasting complex datasets, our OLS model is computationally easy to handle. This computational efficiency is particularly useful when utilizing a blocked cross-validation scheme for forecasting long time series since this approach requires fitting the model and forecasting many times (one time for each cross-validation split). We also observe that, while the proposed method may not be considered a real-time prediction method, it nevertheless generates accurate forecasts quickly on a daily basis, and it could be easily adapted to generate forecasts more frequently (for example, every hour). In addition to its computational efficiency, other advantages of the proposed OLS model over more complex approaches are its flexibility in adding external information (e.g., dummy variables to capture holiday information or different traffic management strategies) and its interpretability. Note that in this study we did not consider external information such as holidays directly in the model, because of our goal of detecting traffic anomalies. We observe that, although the results presented in this paper concern a static model (i.e., the same predictors for all cross-validation splits), the model could be updated and adapted to capture the latest changes in time series patterns. Our proposed model also has the practical advantage of handling missing values by simply automatically removing them, while models like ARIMA require imputation.

Earlier detection of unusual traffic events is critical for traffic authorities' decision-making to maintain smooth mobility. Results of this study can be easily updated daily (or hourly), which can be very valuable to the national freeway bureau for preventing traffic jams and congestion as well as for improving management policies. While we applied the OLS model for forecasting and anomaly detection on Taiwanese highways, this model can also be applied to areas with more complex road structures and a higher number of road divisions. Indeed, the OLS model remains computationally efficient even with an increased number of time series, whereas models like ARIMA experience linear increases in computation time as the number of series grows (Ashouri et al., 2021).

6 Funding

F. K. H. Phoa acknowledges the support of the Academia Sinica (Taiwan) grant number AS-IA-112-M03, and the National and Science Council (Taiwan) grant number 111-2118-M-001-007-MY2. M.A. Cremona acknowledges the support of the Natural Sciences and Engineering Research Council of Canada (NSERC), of the Fonds de recherche du Québec Health (FRQS), and of FSA, Université Laval.

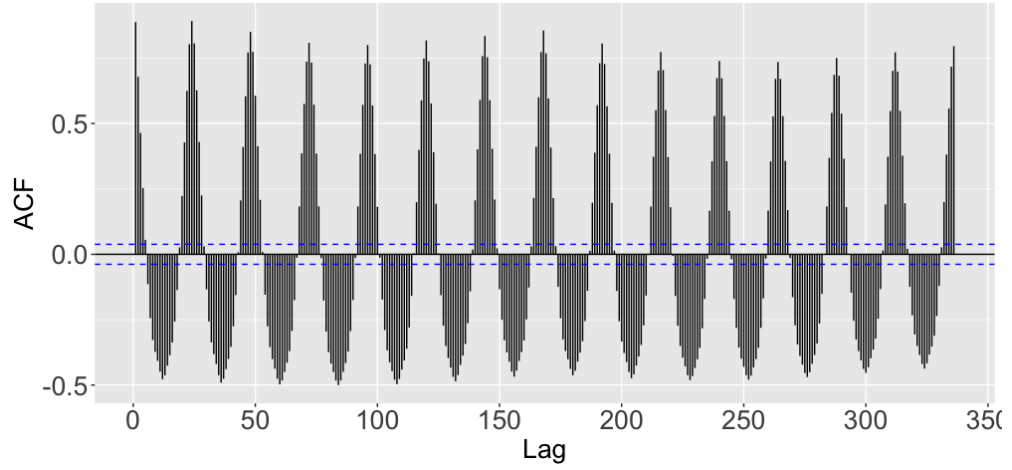
References

- Aboah, A. (2021). A vision-based system for traffic anomaly detection using deep learning and decision trees. In *Proceedings of the IEEE/CVF Conference on Computer Vision and Pattern Recognition*, pages 4207–4212.
- Ashouri, M., Cai, K., Lin, F., and Shmueli, G. (2018). Assessing the value of an information system for developing predictive analytics: The case of forecasting school-level demand in taiwan. *Service Science*, 10(1):58–75.
- Ashouri, M., Hyndman, R. J., and Shmueli, G. (2021). Fast forecast reconciliation using linear models. *Journal of Computational and Graphical Statistics*, pages 1–20.
- Ashouri, M., Shmueli, G., and Sin, C.-Y. (2019). Tree-based methods for clustering time series using domain-relevant attributes. *Journal of Business Analytics*, 2(1):1–23.
- Bawaneh, M. and Simon, V. (2019). Anomaly detection in smart city traffic based on time series analysis. In *2019 International Conference on Software, Telecommunications and Computer Networks (SoftCOM)*, pages 1–6. IEEE.
- Chu, C., Hu, S.-R., Chiang, C., and Lu, Y. (2015). Road space rationing policies for freeway holiday congestion management in taiwan-a simulation approach. In *20th International Conference of Hong Kong Society for Transportation Studies: Urban Transport Analytics, HKSTS 2015*, pages 287–293. Hong Kong Society for Transportation Studies Limited.
- Davison, A. C. and Hinkley, D. V. (1997). *Bootstrap methods and their application*. Number 1. Cambridge university press.
- Djenouri, Y., Belhadi, A., Lin, J. C.-W., Djenouri, D., and Cano, A. (2019). A survey on urban traffic anomalies detection algorithms. *IEEE Access*, 7:12192–12205.

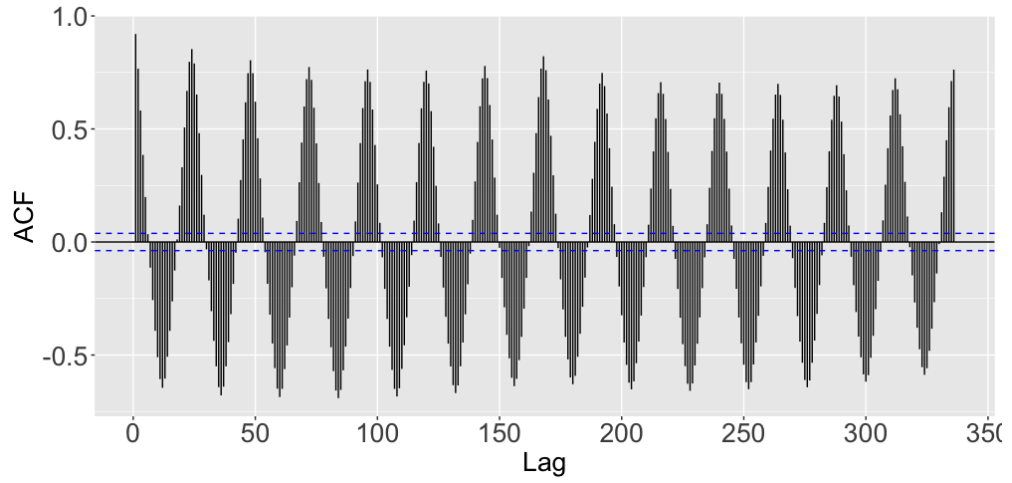
- Gross, C. W. and Sohl, J. E. (1990). Disaggregation methods to expedite product line forecasting. *Journal of Forecasting*, 9(3):233–254.
- Hou, D., He, H., Huang, P., Zhang, G., and Loaiciga, H. (2013). Detection of water-quality contamination events based on multi-sensor fusion using an extended dempster-shafer method. *Measurement Science and Technology*, 24(5):055801.
- Huang, T., Liu, C., Sharma, A., and Sarkar, S. (2018). Traffic system anomaly detection using spatiotemporal pattern networks. *International Journal of Prognostics and Health Management*, 9(1).
- Hyndman, R. J., Ahmed, R. A., Athanasopoulos, G., and Shang, H. L. (2011). Optimal combination forecasts for hierarchical time series. *Computational Statistics & Data Analysis*, 55(9):2579–2589.
- Hyndman, R. J. and Athanasopoulos, G. (2018). *Forecasting: principles and practice*. OTexts, Melbourne, Australia.
- Hyndman, R. J. and Khandakar, Y. (2008). Automatic time series forecasting: the forecast package for r. *Journal of statistical software*, 27:1–22.
- Kahn, K. B. (1998). Revisiting top-down versus bottom-up forecasting. *The Journal of Business Forecasting*, 17(2):14.
- Li, X., Zhang, T., and Liu, Y. (2019a). Detection of voltage anomalies in spacecraft storage batteries based on a deep belief network. *Sensors*, 19(21):4702.
- Li, Z., Zheng, Z., and Washington, S. (2019b). Short-term traffic flow forecasting: a component-wise gradient boosting approach with hierarchical reconciliation. *IEEE Transactions on Intelligent Transportation Systems*, 21(12):5060–5072.
- Mondal, M. A. and Rehena, Z. (2020). Road traffic outlier detection technique based on linear regression. *Procedia Computer Science*, 171:2547–2555.
- Pang, J., Liu, D., Peng, Y., and Peng, X. (2018). Optimize the coverage probability of prediction interval for anomaly detection of sensor-based monitoring series. *Sensors*, 18(4):967.
- Riveiro, M., Lebram, M., and Elmer, M. (2017). Anomaly detection for road traffic: A visual analytics framework. *IEEE Transactions on Intelligent Transportation Systems*, 18(8):2260–2270.
- Siu, K. T., Xu, Y., Tai, Y. M., Choi, T., Michael Wong, K., and To, K. (2020). Switching behavior and control policy of congestion: Examples from taiwan highway system. *New Mathematics and Natural Computation*, 16(03):657–667.
- Tang, S. and Gao, H. (2005). Traffic-incident detection-algorithm based on nonparametric regression. *IEEE Transactions on Intelligent Transportation Systems*, 6(1):38–42.
- Wickramasuriya, S. L., Athanasopoulos, G., and Hyndman, R. J. (2019). Optimal forecast reconciliation for hierarchical and grouped time series through trace minimization. *Journal of the American Statistical Association*, 114(526):804–819.
- Zhang, Z., He, Q., Tong, H., Gou, J., and Li, X. (2016). Spatial-temporal traffic flow pattern identification and anomaly detection with dictionary-based compression theory in a large-scale urban network. *Transportation Research Part C: Emerging Technologies*, 71:284–302.

A Additional data exploration

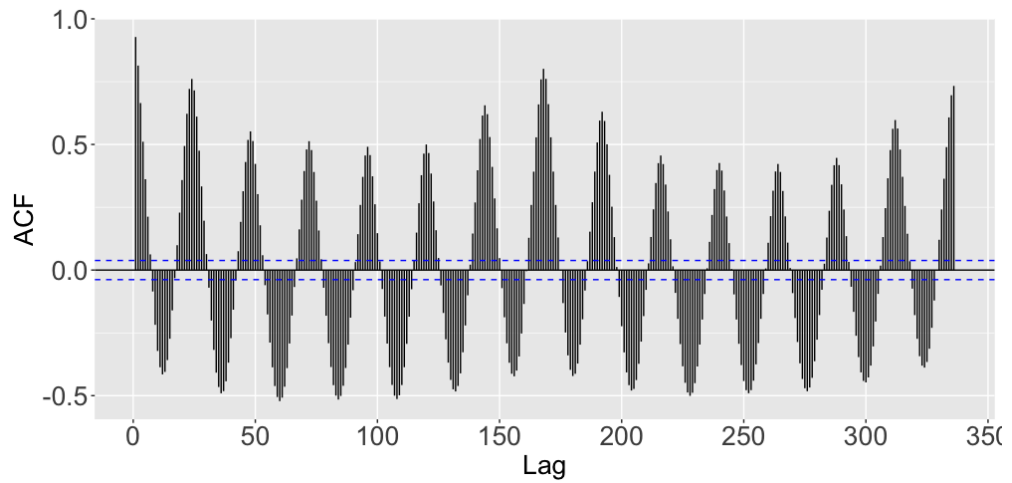
Figures 11 and 12 display the Autocorrelation functions (ACF) and the Partial Autocorrelation functions (PACF), respectively, for three examples of Taiwanese highway hourly time series (from 2021-04-16 23:00:00 to 2021-04-30 22:00:00 - last two weeks) in three regions for different stations, traffic directions, and vehicle types (the same series plotted in Figure 2). Figure 11 shows a clear seasonal pattern in the data in all the three series, corresponding to lag 24, i.e. to a period of 1 day. This suggests that incorporating daily patterns into the data modeling process is appropriate (i.e., using Fourier terms with a period of 24 hours in the OLS model). Figure 11c also shows an additional seasonal pattern with a period of one week (i.e., with lag $168 = 7 \times 24$ hours). This seasonality seems present, although much less pronounced, also in the other two series (Figures 11a and 11b), emphasizing the necessity of incorporating also a weekly periodicity when modeling the data (i.e., using Fourier terms with a period of 7×24 hours in the OLS model). Figure 12 shows a significant spike at lag 1, whereas the lowest significant values occur at lags 2 and 24. These results suggest that utilizing lags 1 and 24 to capture autocorrelation in the OLS model is suitable.



(a) Northern region, Zhongli runway - Hukou, south direction, car

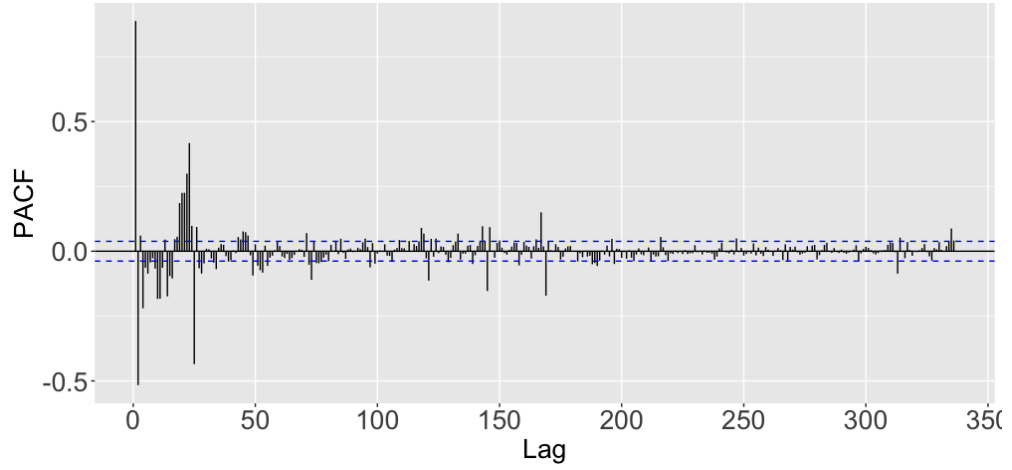


(b) Central region, Xiangshan - Xibin, south direction, small truck

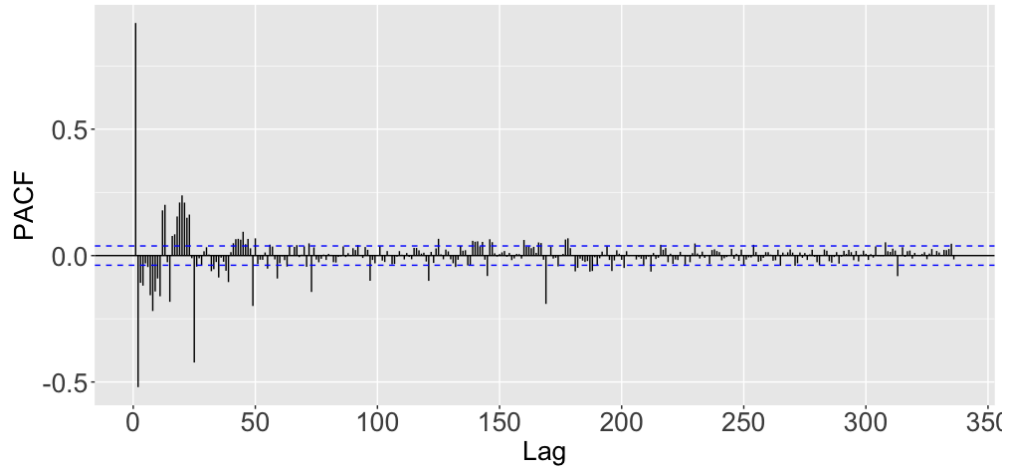


(c) Southern region, Yanchao SIC - Tianliao, north direction, big truck

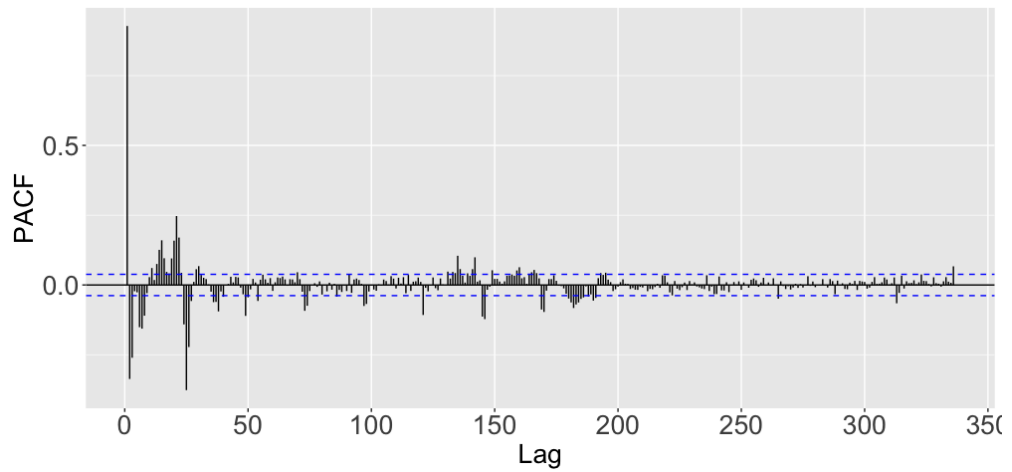
Figure 11: ACF and PACF plots on examples of Taiwanese highway hourly time series (from 2021-04-23 23:00:00 to 2021-04-30 22:00:00) in three regions for different stations, traffic directions, and vehicle types.



(a) Northern region, Zhongli runway - Hukou, south direction, car



(b) Central region, Xiangshan - Xibin, south direction, small truck



(c) Southern region, Yanchao SIC - Tianliao, north direction, big truck

Figure 12: PACF plots on examples of Taiwanese highway hourly time series (from 2021-04-23 23:00:00 to 2021-04-30 22:00:00) in three regions for different stations, traffic directions, and vehicle types.

B Additional analysis of anomalies

Table 7 shows the anomaly counts per day (divided by holiday length) of each holiday in each of the three highways and in four directions. The table comprises four time intervals within a day, namely: 00:00 to 05:00, 06:00 to 11:00, 12:00 to 17:00, and 18:00 to 23:00. The same information is depicted in Figure 13.

Table 7: Number of detected anomalies per day (divided by holiday length) in the 18 long holidays in highways No.1, Elevated No.1, and No.3 in the north, south, east, and west directions, divided into four time intervals: 00:00-05:00 (1), 06:00-11:00 (2), 12:00-17:00 (3), and 18:00-23:00 (4). Cell background colors are proportional to the number of anomalies detected (white for 0-1.5 anomalies, light gray for 1.5-3 anomalies, gray for 3-4.5 anomalies, and dark gray for 4.5 or more anomalies).

Holiday	North direction												South direction												East direction				West direction																																																																																																																																																																																																																																																																																																																																																																																																																																																																																																																																																																																																																																																																																																																																																																																																																																																																																																																																																																																																																																																																																																																																																																																																																																																																																					
	No.1				Elevated No.1				No.3				Elevated No.1				No.1				Elevated No.1				No.3				Elevated No.1				No.1				Elevated No.1																																																																																																																																																																																																																																																																																																																																																																																																																																																																																																																																																																																																																																																																																																																																																																																																																																																																																																																																																																																																																																																																																																																																																																																																																																																																													
	1	2	3	4	1	2	3	4	1	2	3	4	1	2	3	4	1	2	3	4	1	2	3	4	1	2	3	4	1	2	3	4	1	2	3	4	1	2	3	4																																																																																																																																																																																																																																																																																																																																																																																																																																																																																																																																																																																																																																																																																																																																																																																																																																																																																																																																																																																																																																																																																																																																																																																																																																																																										
2019																																																																																																																																																																																																																																																																																																																																																																																																																																																																																																																																																																																																																																																																																																																																																																																																																																																																																																																																																																																																																																																																																																																																																																																																																																																																																																																		</

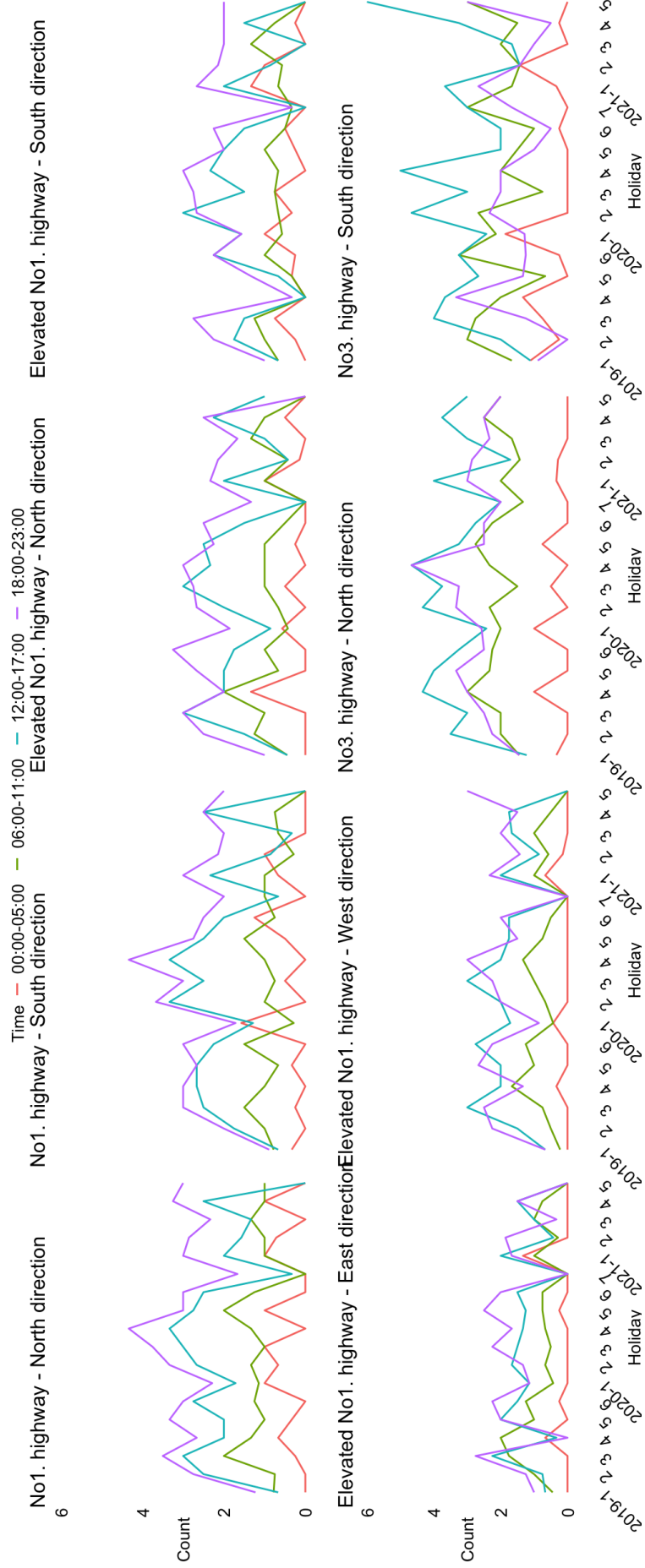


Figure 13: Number of detected anomalies per day (divided by holiday length) in the 18 long holidays in highways No.1, Elevated No.1, and No.3 in the north, south, east, and west directions, divided in four time intervals: 00:00-05:00 (1), 06:00-11:00 (2), 12:00-17:00 (3), and 18:00-23:00 (4).